ACS APPLIED MATERIALS & INTERFACES

Research Article

www.acsami.org

Rate-Dependent, Li-Ion Insertion/Deinsertion Behavior of $LiFePO_4$ Cathodes in Commercial 18650 $LiFePO_4$ Cells

Qi Liu,[†] Hao He,[†] Zhe-Fei Li,[†] Yadong Liu,[†] Yang Ren,*[,‡] Wenquan Lu,[§] Jun Lu,[§] Eric A. Stach,[⊥] and Jian Xie*[,†]

[†]Department of Mechanical Engineering, Purdue School of Engineering and Technology, Indiana University–Purdue University, Indianapolis, Indiana 46202, United States

[‡]X-ray Science Division, Advanced Photon Source, and [§]Chemical Science and Engineering Division, Argonne National Laboratory, 9700 South Cass Avenue, Lemont, Illinois 60439, United States

[⊥]Center for Functional Nanomaterials, Brookhaven Laboratory, Upton, New York 11973, United States

Supporting Information

ABSTRACT: We have performed operando synchrotron high-energy X-ray diffraction (XRD) to obtain nonintrusive, real-time monitoring of the dynamic chemical and structural changes in commercial 18650 $LiFePO_4$/C cells under realistic cycling conditions. The results indicate a nonequilibrium lithium insertion and extraction in the $LiFePO_4$ cathode, with neither the $LiFePO_4$ phase nor the $FePO_4$ phase maintaining a static composition during lithium insertion/extraction. On the basis of our observations, we propose that the $LiFePO_4$ cathode simultaneously experiences both a two-phase reaction mechanism and a dual-phase solid-solution reaction mechanism over the entire range of the flat voltage plateau, with this dual-phase solid-solution behavior being strongly dependent on charge/discharge rates. The proposed dual-phase solid-solution mechanism may explain the remarkable rate capability of $LiFePO_4$ in commercial cells.

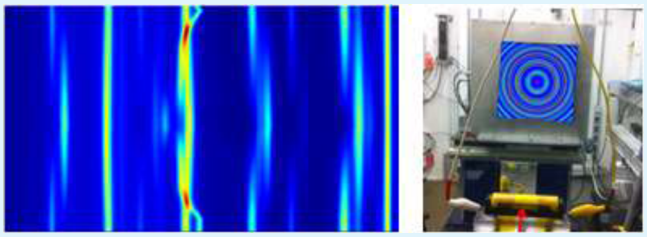

KEYWORDS: *lithium insertion/deinsertion mechanism, lithiation/delithiation $LiFePO_4$, synchrotron high-energy X-ray diffraction, commercial cells,*

1. INTRODUCTION

Because of its high safety rating, long cycle life, low toxicity, and low cost, lithium iron phosphate ($LiFePO_4$) is considered to be one of the most promising cathode materials for lithium-ion batteries (LIBs), with numerous applications in transportation (i.e., for hybrid electric vehicles (HEVs) and electric vehicles (EVs)), portable electronics (i.e., cell phones, laptops, etc.), and power tools. In the past 20 years, significant effort has been devoted to improving the performance of $LiFePO_4$, e.g., using a carbon coating layer on the surface of $LiFePO_4$ nanoparticles,[1−3] doping it with transition metals to increase the electronic conductivity,[4,5] and reducing particle size to shorten the lithium-ion diffusion length.[3] On the basis of these improvements, A123 Systems has developed commercial 18650 $LiFePO_4$/C LIB cells with excellent cycle life[6] and outstanding rate performance.[7]

Although the performance of $LiFePO_4$ has been improved significantly, the underlying mechanism of lithium-ion insertion and deinsertion in $FePO_4$/$LiFePO_4$ (FP/LFP) is still not clearly understood.[8−10] Specifically, the effect of phase changes, if any, on the rate performance of the $LiFePO_4$ cathodes has not been addressed. Extensive efforts have been devoted to understanding the phase transformations that occur in $LiFePO_4$ during the lithium ion insertion and deinsertion process.[11−15] Several possible mechanisms have been proposed, including a core–shell model,[16] a mosaic model,[17] and a shrinking-core model,[17] each of which has had – to some extent – success in explaining the lithium-ion insertion/deinsertion process. However, none of these models can completely explain the high rate performance that is observed in $LiFePO_4$ cathodes, indicating that these models need further refinement. Indeed, Laffont et al.[18] recently provided experimental evidence that the interface between single-phase areas is not a solid solution, but rather the juxtaposition of the two final states, fully discharged $LiFePO_4$ and fully charged $FePO_4$, thereby providing experimental evidence which invalidated the core–shell model. However, another completely different model – the "domino-cascade model" – has been proposed by Delmas et al.,[19] who used ex situ XRD and electron microscopy to conclude that the Li-ion extraction process is limited by $LiFePO_4$ nucleation instead of Li^+ diffusion. The reason behind these inconsistent and sometimes contradictory models is primarily due to the lack of effective operando techniques that

Received: November 19, 2013
Accepted: February 12, 2014
Published: February 12, 2014

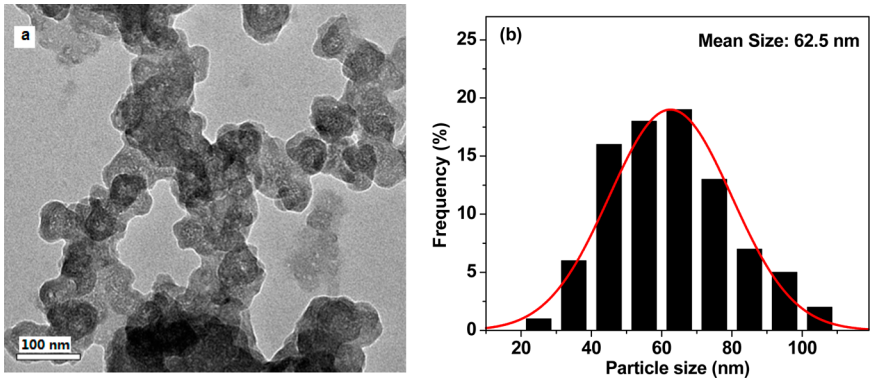

Figure 1. (a) Transmission electron microscopy image of the $LiFePO_4$ cathode. (b) Particle size distribution of $LiFePO_4$ particles.

monitor the phase changes that occur in $LiFePO_4$ as the lithium-ion insertion and extraction process is occurring.[20]

Theoretically, the availability of a single-phase transformation path during lithium insertion and extraction have been predicted at a very low overpotential,[13] which suggests the existence of a single-phase, solid-solution pathway during battery operation, thereby relating the lithium insertion/extraction mechanism to the remarkable rate capacity of $LiFePO_4$. Indeed, a single-phase solid-solution Li insertion/extraction process was observed to occur in electrodes made of $LiFePO_4$ nanoparticles (40 nm), as evidenced by a continuous shift of the diffraction peaks during charge/discharge.[21] However, in the experimental work mentioned above, information regarding the structural evolution of $LiFePO_4$/$FePO_4$ during the lithium insertion/extraction processes was obtained using either coin cells or very small laboratory-scale devices.[13,22,23] Considering the significantly higher loading of active material in a commercial 18650 cell, it is possible the cell performance in the commercial cell might be different from that which occurs in the coin cell, and may in fact alter the lithium insertion/extraction mechanism.

There are two basic mechanisms occurring during charge and discharge: (1) a solid-solution reaction mechanism in which only one phase (i.e., $Li_{1-x}FePO_4$) exists during the charging/discharging process and (2) a two-phase reaction mechanism, in which the $LiFePO_4$ phase is transformed directly through a first-order phase transition into the $FePO_4$ phase as the charging proceeds, with the $FePO_4$ phase being transformed back into $LiFePO_4$ phase during the discharge process. In the first case – the solid solution reaction – only a single phase is involved, and as a result the lattice parameters and unit-cell volumes would be expected to change continuously during the charge/discharge cycle.[21,24] In the second case – associated with a first-order phase transition – the unit-cell volumes of both phases remain nearly constant, with the unit cell volume difference of two phases varying by only $\Delta V = 6.5\%$. The distinct nature of these two mechanisms is thus apparent using X-ray diffraction, and as a result, this technique is particular amenable to revealing the underlying mechanisms.

We have investigated the structural changes that occur in $LiFePO_4$ electrodes in commercial 18650 cells during the charge/discharge process using operando synchrotron high-energy XRD. High-energy synchrotron X-rays with a photon energy of 115 keV are capable of penetrating through thick samples, which allowed us to probe commercial 18650 cells during operation, without any cell modification. In addition, employing a fast XRD scan directly during cycling of the Li-ion battery cells provides a nonintrusive, real-time monitoring of the changes that occur within the electrodes under real operating conditions: this is critical for elucidating the mechanism of Li^+ insertion/extraction. We demonstrate that a nonequilibrium lithium insertion and extraction occurs in $LiFePO_4$/$FePO_4$ during the charge/discharge of a commercial 18650 cell, with neither the $LiFePO_4$ phase nor the $FePO_4$ phase maintaining a constant unit cell volume during lithium insertion/extraction. The single-phase solid-solution transformation path of lithium insertion/extraction for both the $LiFePO_4$ phase and the $FePO_4$ phase exists at different cycling rates, which is surprisingly concurrent with the two-phase reaction throughout the flat voltage plateau. This "dual-phase solid-solution" behavior is shown to be dependent on the charge/discharge rates. Consequently, we believe that the remarkable rate capability of $LiFePO_4$ in a commercial cell may be strongly correlated to the existence of this heretofore unobserved dual-phase solid-solution behavior.

2. EXPERIMENTAL SECTION

2.1. Battery. The 18650 cells (APR18650M, 1.1Ah) were provided by A123 Systems with a graphite anode, a $LiFePO_4$ cathode, and a 1.20 M $LiPF_6$ in EC: EMC electrolyte. Importantly, all cells used in the experiment are from the same batch which ensures that all materials and manufacturing condition are the same. No special modification was needed for the 18650 cells before characterization.

2.2. Electrochemical Measurements. Before characterization of in situ high-energy XRD, each cell was completely discharged using a four-channel material and cell test system (MACCOR, U.S.). Four equivalent cells have been cycled and in situ characterized under different cycling rates from 0.1*C*, 1*C*, 3*C*, to 5*C*. For the cell cycled at the 1*C* rate. the cell was charged to 3.60 V at a 1*C* rate (constant current of 1.10 A); the charging was continued at a constant voltage of 3.60 V until the current was <0.02 A, which is regarded as a 100% state of charge (SOC) or 0% depth of discharge (DOD). Then, the cell was discharged at a 1*C* rate until the voltage reached 2.00 V, which is the discharge cutoff voltage of the cell (the corresponding capacity is 1100 mAh). This procedure is considered to be a 100% depth of discharge (DOD). A constant current (1.1 A) was applied to discharge the cell to 2.0 V. Other equivalent cells will perform the same procedure but at different cycling rates as that at 1*C*.

2.3. Characterization. High-resolution TEM characterization was performed with a JEOL 2100F (Japan) operated at 200 kV. In situ time-resolved high-energy XRD measurements during cycling were performed on the beamline 11-ID-C at the Advanced Photon Source, Argonne National Laboratory. A monochromator with a Si (113) single crystal was used to provide an X-ray beam with the energy of 115 keV. High-energy X-ray with a beam size of 0.2 mm × 0.2 mm and wavelength of 0.10798 Å was used to obtain two-dimensional (2D) diffraction patterns in the transmission geometry. X-rays were

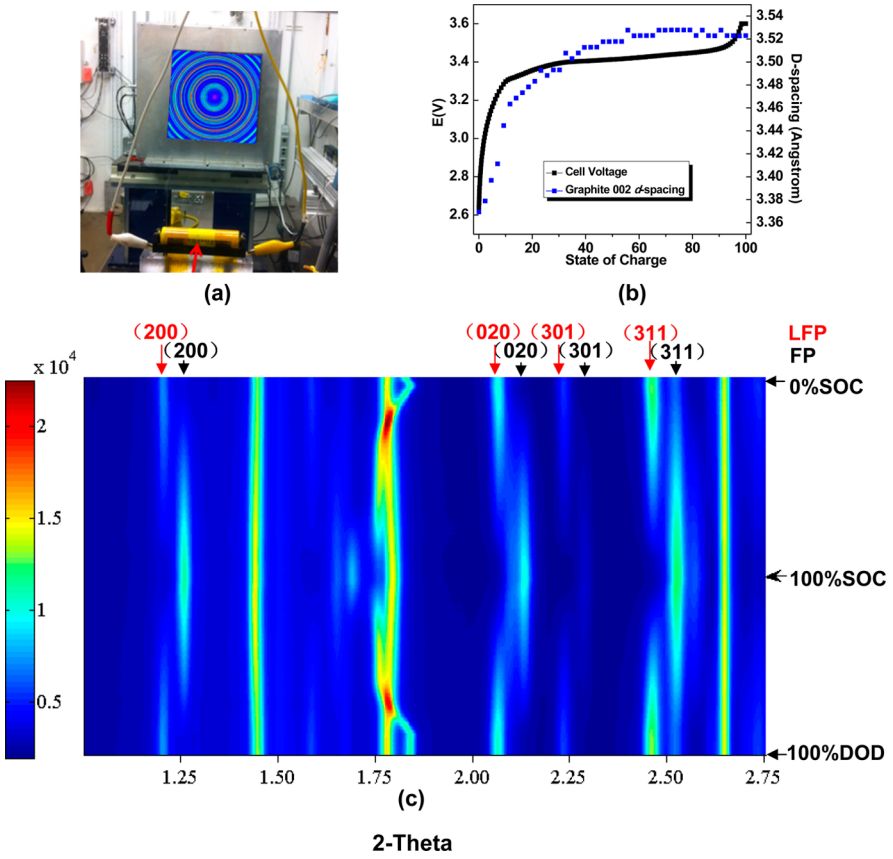

Figure 2. (a) Experiment setup for operando synchrotron high-energy X-ray diffraction (XRD) during electrochemical lithium insertion/extraction. (b) Plot of the *d*-spacing value of graphite (002) and voltage during the charge process at a 1 *C* rate. (c) Contour plot of peak intensities as a function of reaction time throughout the first charge/discharge cycle.

collected with a Perkin-Elmer large-area detector placed at 1800 mm from the sample. Such a high-energy beam provides easy penetration through the stainless steel case of the 18650 cells and offers high-resolution signals and rapid detection of the structural changes of the electrodes. Use of such a beam on an 18650 cell also results in a very high S/N ratio because of the large amount of electrode materials being analyzed inside the cell (cell capacity: 1.0 Ah). The diffraction data was collected every 34 s. The obtained 2D diffraction patterns were calibrated by using a standard CeO_2 sample and converted to 1D patterns using Fit2D software.

3. RESULTS AND DISCUSSION

3.1. Battery and Characterization Methods. Commercial $LiFePO_4$ 18650 cells were provided by A123 Systems. No special modification was made to these cells. As illustrated in Figure 1a, a TEM image of the scattered particles of $LiFePO_4$ extracted from equivalent cells shows that the cathode material exhibits different geometric shapes, primary particles, and agglomerated primary particles and not very broad particle size distribution with the average particle size around 62.5 nm ± 20 nm, as shown in Figure 1b.

The experimental setup for the time-resolved high energy XRD is illustrated in Figure 2a. An A123 18650 $LiFePO_4$ cell was placed on the stage of the beamline and the high-energy beam was penetrated through the whole cell from one side of the cylinder (4.5 mm from the top toward to the center) to another side (Figure.2a). The two-dimensional XRD patterns were converted to a conventional intensity vs 2θ angle plot using the Fit2D program.[25] A full HE-XRD pattern of the 2θ angle from 0 to 9° at the wavelength of 0.10804 Å covers an equivalent 2θ angle range from 0 to 200° for Cu K-α laboratory X-rays with a wavelength of 1.54 Å. Because high-energy X-rays penetrate through the whole cell, diffraction patterns of all of the crystalline materials in the 18650 cell were present in the single diffraction pattern (Figure S1 in the Supporting Information). A contour plot of these diffraction patterns between 2θ = 1.0 and 2.9° shows changes of some characteristic peaks of both the $LiFePO_4/FePO_4$ cathode and the graphite anode during a charge/discharge cycle (Figure 2c). The intensity of the diffraction peaks corresponds to the color scale (on the left). The diffraction patterns are nearly symmetric along the 100% state of charge (SOC) during both charging and discharging, which indicates that Li-ion insertion and deinsertion follow the same mechanism, and that the structural change of the electrodes during the charge/discharge process is reversible. Detailed XRD patterns between 2θ = 1.0° and 2.9° during the charging process at a 1 C rate are shown in Figure S2, Supporting Information. During the charging process, lithium ions deintercalated from the $LiFePO_4$, forming $FePO_4$, and intercalated into graphite, forming lithiated graphite. As mentioned above, many characteristic peaks of $LiFePO_4/FePO_4$ can be clearly identified within the 2θ angles from 1.0 to 2.9°. The triphylite $LiFePO_4$ and heterosite $FePO_4$ phases have the *Pnma* symmetry with slightly different lattice parameters. The anode material is mainly composed of graphite. During the charge process, the 2θ value of the graphite (002) reflection decreased as the lithium ions intercalated into the graphite layer (i.e., SOC increases) to form lithiated graphite. The peak at 2θ = 1.836° in the pattern

at SOC = 0% can be attributed to diffraction from the (002) graphite planes. This peak shifts left to 2θ = 1.754° at SOC = 100%, indicating that the graphite has become lithiated.

The *d*-spacing of the graphite layers can be calculated from the graphite (002) peak and is shown in Figure 2b. The *d*-spacing increased sharply from 3.3741 Å to 3.5128 Å at the first stage of the charging process. The *d*-spacing of 3.5128 Å from the (002) reflection corresponds to the stage-2 compound LiC_{12}. Upon reaching a 50% SOC, the (002) peak intensity decreased with further charging, accompanied by the initiation of a broad peak at 2θ = 1.67° resulting from the formation of the stage-1 compound LiC_6. The phase changes that occur in graphite during charging has been studied extensively by Dahn et al.,[26,27] who provided the phase diagram of Li_xC in great detail, and by Wang et al. using in situ neutron diffraction.[28] Our data is consistent with these studies. Hence, we focused on the structural evolution of the cathode materials during the charge/discharge process.

In our data analysis, the general structure analysis software (GSAS) program was used to fit the observed diffraction patterns, which contained multiple phases. Excellent fitting results were obtained, and as an example, the pattern taken in operando at 20% SOC, is shown in detail in Figure 3. The

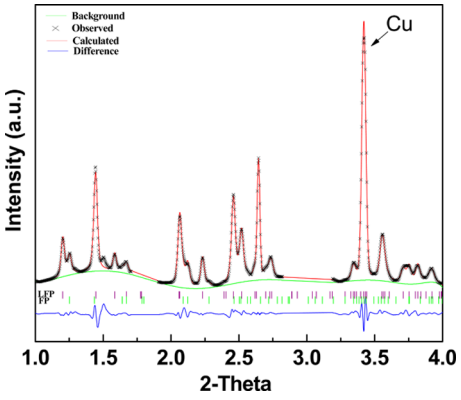

Figure 3. Synchrotron X-ray diffraction patterns taken in operando at the 20% SOC (λ = 0.10804 Angstrom). The standard XRD patterns of $LiFePO_4$ and $FePO_4$ have been given for comparison. The position of the reflections around 3.47° is a result of the Cu foil.

standard reflections of $LiFePO_4$ and $FePO_4$ are indicated for comparison. The reflection at 3.47° is from the Cu foil. The diffracted intensity from the lithiated/delithiated graphite, current collectors (alumina, copper), and casing (iron) were removed during the fitting process.

3.2. Phase Fraction Evolution during the Charge/Discharge Process with Different Rates. As the battery cell was charged (SOC increased), the diffraction peaks of the triphylite $LiFePO_4$ phase gradually transformed into the corresponding peaks of the heterosite $FePO_4$ phase. Because the (200) reflection of $LiFePO_4$ was well-separated from the (200) reflection of $FePO_4$, we were able to use the intensity ratio of this pair of characteristic peaks to establish the phase fraction change during the charge/discharge process, obtained using Rietveld analysis and Gaussian fits to the (200) pair peaks. The normalized phase fractions of triphylite $LiFePO_4$ and heterosite $FePO_4$ as a function of cell voltages are shown in Figure 4, for both the 1*C* and the 0.1*C* charge/discharge cycles. It was found that a single phase (heterosite or triphylite) could be detected only at the beginning or the end of the charge/

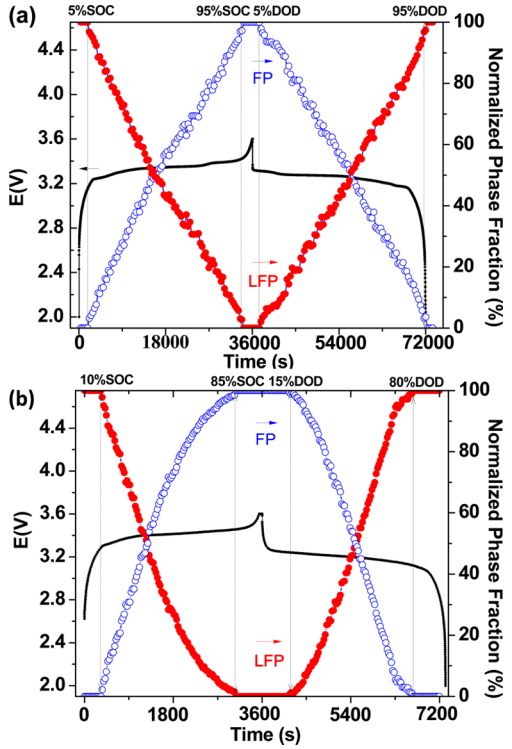

Figure 4. (a) Phase fraction evolution during charge−discharge of the 1st cycle at 0.1 *C*, (b) phase fraction evolution during charge−discharge of the 1st cycle at 1 *C*. Filled circles correspond to LFP ($LiFePO_4$); empty circles correspond to FP ($FePO_4$).

discharge process, while the two phases coexisted in the range of the flat voltage plateau (Figure 4a, b). The change in the phase fraction of triphylite and heterosite at 1*C* and 0.1*C* were found to be quite different. At 0.1*C* a single-phase $LiFePO_4$ region was initially observed between 0 and 5% SOC; thereafter the $FePO_4$ phase appeared after ∼5% SOC and the phase fraction increased with increasing charge. The $LiFePO_4$ phase decreased with charging and disappeared at 95% SOC; finally, a single-phase $FePO_4$ region appeared between 95 and 100% SOC (Figure 4a). The opposite sequence of phase formation occurred during the discharging process (Figure 4a), indicating that the charge/discharge process is completely reversible.

The changes in phase fraction that occurred during the charging/discharging process clearly show the coexistence of both the triphylite and heterosite phases, except at the beginning and the end of the charge/discharge (∼5% SOC range). In addition, in the two-phase region, the phase fraction exhibited a linear change with the SOC, suggesting an ideal two-phase behavior at 0.1 C (Figure 4a), which is consistent with Meethong's study.[29] At the higher 1*C* rate, the phase fraction change with the SOC exhibited a slightly nonlinear behavior at the end of two phase region (Figure 4b). Meanwhile, the single-phase region extended from 0 to 5% SOC at 0.1*C* to 0−10% SOC at 1 C (for $LiFePO_4$) and from 95 to 100% SOC at 0.1*C* to 85−100% SOC at 1.0*C* (for $FePO_4$) during the charge process, whereas the opposite observed for the discharge processes (Figure 4a, b). In particular, for the charge and discharge processes at 1*C* rate, there is slightly asymmetric behavior of the phase fraction for the two phase region during the charge and discharge processes as the two phase regions are compressed into the region of 10−85% SOC in charge process and 15%-80% DOD (Figure.4b) in discharge

dx.doi.org/10.1021/am405150c | ACS Appl. Mater. Interfaces 2014, 6, 3282−3289

process compared to the region of 5−95% SOC and 5−95% DOD at 0.1C rate (Figure 4a), respectively. Also, there is slightly nonlinear behavior of the curves of both FP and LFP at the end of the two phase region during the charge process and at the beginning/end of the two phase region during the discharge process, respectively. Given the consideration that the phase transition delays observed by XRD for $LiFePO_4$ may happen,[30] here, it is believed that the asymmetric behavior at higher rate, 1C, charge and discharge, may result from the lack of the time for relaxation of the FP during the discharge. In this work, the cell was discharged right after charge without any rest, hence, there is no time allowed for FP to relax after lithiation. Under such operating condition, the FP may not need time to relax at 0.1C rate charge/discharge because the system is not too far away from the equilibrium state. However, at a 1C rate, the system is far away from the equilibrium state, hence, the asymmetric behavior is exhibited. We found that the phase fraction change with time during the discharge process behaves more symmetric if the cell is allowed to rest for a period of time after the charge (data not shown here). Please note that the variations of the $LiFePO_4$ and $FePO_4$ phase fractions during the charge/discharge process indicate that a two-phase reaction occurs concomitant with the plateau in voltage.[16,29] In addition, the range over which the single-phase region persisted was significantly larger at the higher charge/discharge rate. This is an additional important finding, and will be discussed in more detail below.

3.3. Unit-Cell Volumes and Lattice Parameter Evolution during the Charge/Discharge Process with Different Rates. The unit cell volumes (determined from GSAS refinements of the two structures) of both $LiFePO_4$ and $FePO_4$ were found to change with the reaction time (Figure 5), and we designate $LiFePO_4$ as $Li_{1-x}FePO_4$ (Li-rich triphylite) and $FePO_4$ as Li_yFePO_4 (Li-poor heterosite) in Figure 5 and the discussion hereafter. At the 0.1C rate, at the very beginning of charging process, i.e., between 0 and ~5% SOC, only one phase, the $Li_{1-x}FePO_4$ (Li-rich triphylite) existed (Figure 5a). Thereafter, the unit-cell volume of $Li_{1-x}FePO_4$ (Li-rich triphylite) decreased slowly with the reaction time until 95% SOC, suggesting that the $Li_{1-x}FePO_4$ (Li-rich triphylite) was undergoing a single-phase solid-solution reaction mechanism (the change of unit cell volume with reaction time during charging/discharging process is characteristic of the solid-solution reaction mechanism[21,24]). Meanwhile, the Li_yFePO_4 (Li-poor heterosite) phase starts to emerge after 5% SOC, and its unit cell volume slowly decreased with reaction time to the end of charging process, i.e., 100% SOC, indicating that Li_yFePO_4 (Li-poor heterosite) was also undergoing a single-phase solid-solution reaction mechanism (in the region of 5−100% SOC). Clearly, from our operando synchrotron experiment, in the region of 5−95% SOC (Figure.5a), two separate single-phase solid-solution reactions, both $Li_{1-x}FePO_4$(Li-rich triphylite) and Li_yFePO_4 (Li-poor heterosite), occurred simultaneously at the $LiFePO_4$ cathode system. To differentiate our findings from the conventional single-phase solid-solution reaction mechanism, we call this behavior a "dual-phase" solid-solution reaction mechanism (ie. both the Li_yFePO_4, Li-poor heterosite phase and $Li_{1-x}FePO_4$, Li-rich triphylite phase are present at the same time, but in differing amount). Note that close to the end of the charging process, i.e., between 95 and 100% SOC, only one phase Li_yFePO_4 (Li-poor heterosite) existed. This is different from the findings of Yamada, et al.,

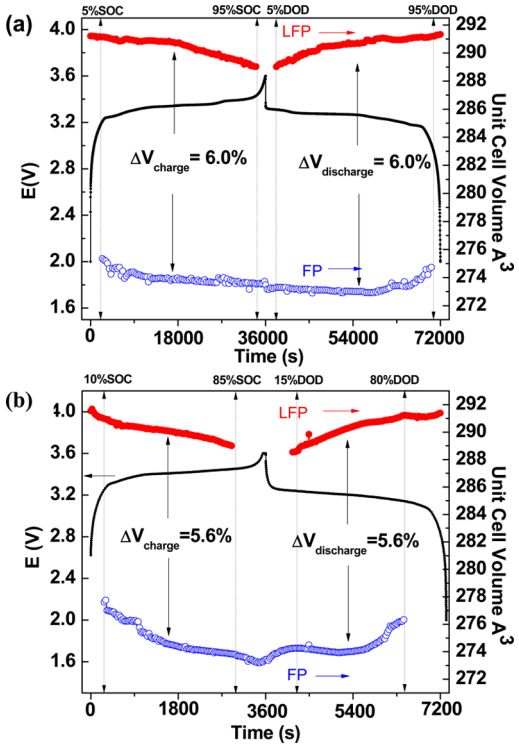

Figure 5. (a) Unit-cell volume evolutions during charge−discharge of the first cycle at 0.1 *C*. (b) Unit-cell volume evolutions during charge−discharge of the first cycle at 1 *C*. Filled circles correspond to LFP (Li-rich triphylite); empty circles correspond to FP (Li-poor heterosite).

which indicated the existence of solid solution only at the very beginning and end of the charging.[31]

On the other hand, even our results show that both $Li_{1-x}FePO_4$ (Li-rich triphylite) and Li_yFePO_4 (Li-poor heterosite) could transform through solid-solution path; however, at the relative low cycling rates, two-phase reaction mechanism still dominates the process.[13] The dual-phase solid-solution behavior was found to be strongly dependent on the cycling rates. For the cell cycled at the 1C rate, within the dual-phase solid-solution region (Figure 5b, i.e., between 10 and 85% SOC), $Li_{1-x}FePO_4$ experienced a similar decrease in the unit cell volume as occurred with the 0.1 C rate discharge, but at a much higher rate. It is noteworthy that at the 1 C rate, the Li_yFePO_4 phase (Li-poor heterosite), which formed during the charging process, possessed a much larger unit-cell volume than the literature reported values[16,29] and exhibited a much faster rate of change in terms of the unit-cell volume. The unit-cell volume difference between the $Li_{1-x}FePO_4$ cell and the Li_yFePO_4 cell changed from ΔV= 6.0% at 0.1 C (Figure 5a) to ΔV = 5.6% at 1C (Figure 5b). This is different from the reported value of 6.5%,[16] the unit-cell volume difference between two end members $LiFePO_4$ and $FePO_4$. We proposed that this difference between our values and the value reported from ref 16. is caused by the existence of an single-phase solid-solution path, as theoretically predicted under nonequilibrium conditions.[13] Meanwhile, in the region of the single-phase solid-solution reaction (0−10% and 85−100% SOC, and 0−10% and 80−100% DOD in Figure 5b), the unit-cell volume of both $Li_{1-x}FePO_4$ and Li_yFePO_4 changed at much higher rates than those at 0.1C (Figure 5a). Interestingly, the behavior of the unit-cell volume change of both $Li_{1-x}FePO_4$ and Li_yFePO_4 phases is almost symmetric during lithiation and delithiation

process at 0.1*C* rate (Figure 5a), whereas at the 1*C* rate, the behavior of the unit-cell volume change for Li_yFePO_4 phase is slightly asymmetric (Figure 5b). During the discharge process, the unit-cell volume slowly increases in the single-phase region, then after enters the two-phase region, slightly decreases (almost like a plateau) and rises up all the way to the end of the two phase region. Bramnik reported that, for $LiCoPO_4$ cathode, the character of structure changes observed at charge and discharge is quite different, it is slightly asymmetric for Li-rich phase while discharge induces a strong increase of the cell volume change for Li-poor phase.[32] For the $LiFePO_4$ system studied here, a similarly asymmetric unit-cell volume change for Li-poor phase may exist especially at the higher rate, which may be ascribed to the lack of time for FP relaxing after charge at higher rate, 1*C*, charge/discharge as we explain the behavior of phase fraction change in Figure 4b in section 3.2.

To further describe the delithiation of $Li_{1-x}FePO_4$ during charging, the lattice parameters of $Li_{1-x}FePO_4$ and Li_yFePO_4 are plotted as a function of reaction time in Figure S3 (Supporting Information). The lattice parameters *a* and *b* of both $Li_{1-x}FePO_4$ and Li_yFePO_4 changed in the same manner as that of the unit-cell volume in Figure 5, with a higher rate at 1 *C* than at 0.1 *C*. However, the lattice parameter *c* remains relatively unchanged. The variation in $Li_{1-x}FePO_4$ and Li_yFePO_4 phase fractions demonstrates the two-phase reaction and the change in $Li_{1-x}FePO_4$ and Li_yFePO_4 lattice parameters indicates the solid solution.[24,33] Considering the phase fraction changes (Figure 4) and the unit cell volume (lattice parameters) changes (Figure 5) at both 0.1*C* and 1*C* rates, it is clear that the $LiFePO_4$ cathode simultaneously experienced both a two-phase reaction and a dual-phase solid-solution reaction over the entire range of the flat voltage plateau. The extent of each reaction mechanism in the charging/discharging process is strongly affected by the charging rate, namely, the applied current density. It is important to note that this is in contrast to prior observation of such phenomenon, which was only observed in a very small voltage region (3.49−3.52 V).[24] Our results show that such coexisting reaction mechanisms occur over the entire range of the flat voltage plateau.

This finding is further supported by Figure 6a, which summarizes the evolution of the unit-cell volume during the discharge process as a function of rate. The change in unit-cell volume with depth of discharge (DOD) became more rapid as the charge/discharge rate increased. The unit-cell volume difference (ΔV) between the $LiFePO_4$ phase and the $FePO_4$ phase decreased with increasing rate of discharge, and was about ΔV = 5.0% at 3*C* and ΔV = 4.8% at 5*C*, much smaller than was observed at lower rates (ΔV = 6.0% at 0.1*C* and ΔV = 5.6% at 1*C*). Importantly, the region of the dual-phase solid solution narrowed with the increased charge/discharge rates (i.e., from the region of 5−95% DOD at 0.1*C* to the region of 20−75% DOD at 5*C*). Eventually, at extremely high rates, it is anticipated that the region of the dual-phase solid solution may be diminished as shown in Figure 6b, which is taken from the extrapolation of the data in Figure 6a. Consequently, this also demonstrates that with increasing charge/discharge rates, the dual-phase solid-solution region will be compressed and the single-phase solid-solution region will be expanded.

To date, the mechanism of the Li^+ ion insertion/extraction in the $LiFePO_4$ electrode has remained a matter of debate. The two-phase growth process[16,18,19,34,35] involves the coexistence of both phases ($LiFePO_4$ and $FePO_4$), which is in contradiction to the solid-solution reaction observed in both $LiFePO_4$

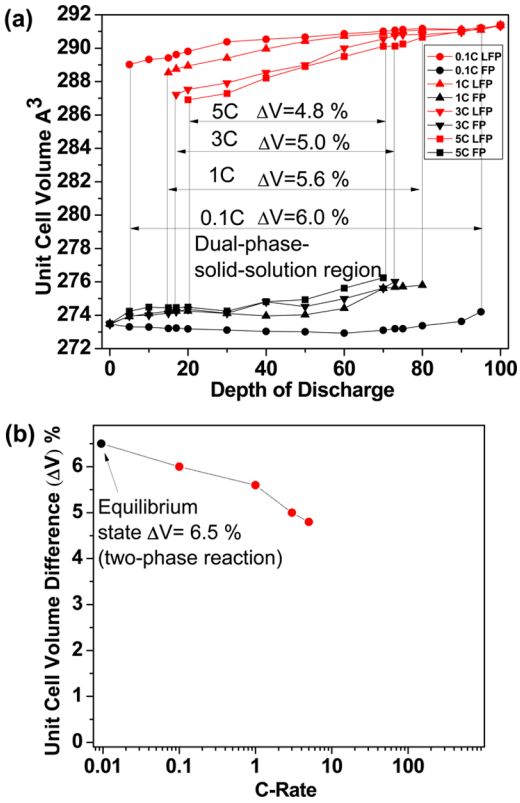

Figure 6. (a) Unit-cell volume evolutions during the discharge process at 0.1*C*, 1*C*, 3*C*, and 5*C*. (b) Unit-cell volume difference (at the entire voltage plateau) vs *C* rate.

nanoparticles[31,36−38] and bulk $LiFePO_4$ materials.[24] Our operando experiment reveals that (1) the phase fractions of both $LiFePO_4$ and $FePO_4$ (Figure 4) change with SOC at both low rates (i.e., 0.1*C*) and high rates (i.e., 1*C*), suggesting that the $LiFePO_4$ electrode is undergoing a two-phase reaction mechanism in the entire flat voltage plateau; (2) the unit-cell volume of both $LiFePO_4$ and $FePO_4$ (Figure 5) changes with the SOC at both low rates (i.e., 0.1*C*) and high rates (i.e., 1*C*), indicating that the electrode is experiencing the dual-phase solid-solution reaction mechanism, and (3) the difference (ΔV) in the unit-cell volume between the $LiFePO_4$ phase and the $FePO_4$ phase reduces as the rate increases (Figure 6), implying that the region over which the dual-phase solid-solution exists will be compressed with increased rates and, eventually, may be diminished at extremely high rates. It is well-known that the insertion and desinertion of Li^+ ion within the $LiFePO_4$ electrode undertake the two-phase pathway whereas the $LiFePO_4$ electrode is charged/discharged at very low rate (i.e., very small overpotential) which is close to the equilibrium state.[13] Under such condition (i.e., close to the equilibrium state), the relaxation of the lattice structure allows the evolution of two-phase structure. In other words, it is more closed to a thermodynamically controlled process. However, as the charge/discharge rate is significantly increased, the insertion/deinsertion process becomes kinetic controlled which does not allow the relaxation of the lattice structure, rather, the homogeneous distribution of $LiFePO_4$ and $FePO_4$ occurs, namely, the solid solution is formed. Hence, the process is dominated by the solid solution pathway.[39] Our results suggest that the insertion/deinsertion process is rate dependent and the two different mechanisms, two-phase and solid-solution, coexist

during the charge/discharge process. At very low overpotential (i.e., very low rate charge/discharge), the process is dominated by the two-phase mechanism while it might be dominated by the solid solution mechanism at very high overpotential (i.e., very high rate charge/discharge). Between the two extremes, the process is controlled by both mechanisms with different ratios depending on the rate.

From points 1 and 2, the conclusion can be drawn that the $LiFePO_4$ cathode experiences a dual-phase solid-solution reaction mechanism over the entire charge/discharge process. In other words, the $LiFePO_4$ cathode in a commercial cell experiences neither an exclusive two-phase reaction mechanism nor an exclusive single-phase solid-solution reaction mechanism. Considering the third point, it can be concluded that the excellent high-rate performance of $LiFePO_4$ cathodes may be attributed to the reduction of the dual-phase solid-solution region and the increase of the single-phase solid-solution region with increasing rate. Compared with the two-phase reaction, the solid-solution reaction transformation path holds a significant advantage: the transformation of Li^+ ions into the $LiFePO_4$ cathode is more facile and homogeneous.[18] In addition, the solid-solution phase existing inside the region of the dual-phase solid solution also helps facilitating the transformation process of Li^+ ions. This is also consistent with what has been theoretically predicted by Bai et al.,[11] namely, that the region of the dual-phase solid solution is compressed with the increased rate, whereas the single-phase transformation region is expanded.

4. CONCLUSION

In summary, the structural changes in a real-world $LiFePO_4$ 18650 cell were investigated using advanced operando synchrotron X-ray diffraction (XRD). The mechanisms of Li ion intercalation in the $LiFePO_4$ cathode were elucidated from the structural changes observed. The $LiFePO_4$ cathode in the commercial 18650 cell undergoes neither a complete two-phase reaction mechanism nor a complete single-phase solid-solution reaction mechanism. Rather, the cathode simultaneously experiences both a two-phase reaction mechanism and a dual-phase solid-solution reaction mechanism over the entire range of the flat voltage plateau. Outside the flat voltage plateau, the cathode still experiences a single-phase solid-solution mechanism in a very small range of SOCs. The observed changes of the dual-phase solid-solution region with DOD may provide an explanation for the excellent rate performance of the $LiFePO_4$ cathode in the commercial 18650 cell. Critically, by exploring the microstructural evolution that occurs in the $LiFePO_4$ electrode of a "real-world" 18650 cell, we have elucidated the Li^+ ion insertion/extraction mechanism in such a way as to maximize the impact on real battery design and application than the results obtained from coin cells or lab cells.

■ ASSOCIATED CONTENT

Supporting Information

A description of the experimental data processing, the analysis, the detailed XRD data, and the additional lattice parameter changes are provided in the Supporting Information. This material is available free of charge via the Internet at http://pubs.acs.org.

■ AUTHOR INFORMATION

Corresponding Author

*(J.X.) E-mail: jianxie@Iupui.edu.

Author Contributions

J.X. designed, guided the project and revised the manuscript. Y.R. guided the use of the HE-XRD and the data analysis. Q.L., Y.R., and H.H. designed and performed the experiments. Q.L. and Y.L. performed the Li-ion battery tests. Q.L. and Z.L. drafted the manuscripts. Q.L. and Y.R. analyzed the experiment data. E.A.S. obtained the TEM images and refined the manuscript.

Notes

The authors declare no competing financial interest.

■ ACKNOWLEDGMENTS

This work was partially supported by the U.S. Navy under Contract N00164-09-C-GS42. The authors would also like to express the appreciation to A123 Systems for providing the 18650 $LiFePO_4$ cells for testing. Use of the Advanced Photon Source was supported by the U.S. Department of Energy, Office of Science, Office of Basic Energy Science, under Contract DE-AC02-06CH11357. This research was also carried out in part at the Center for Functional Nanomaterials of the Brookhaven National Laboratory (U.S. DOE contract DE-AC02-98CH10886).

■ REFERENCES

(1) Mi, C. H.; Zhao, X. B.; Cao, G. S.; Tu, J. P. *J. Electrochem. Soc.* **2005**, *152*, A483−A487.
(2) Sides, C. R.; Croce, F.; Young, V. Y.; Martin, C. R.; Scrosati, B. *Electrochem. Solid-State Lett.* **2005**, *8*, A484−A487.
(3) Wu, X.-L.; Jiang, L.-Y.; Cao, F.-F.; Guo, Y.-G.; Wan, L.-J. *Adv. Mater.* **2009**, *21*, 2710−2714.
(4) Shi, S.; Liu, L.; Ouyang, C.; Wang, D.-s.; Wang, Z.; Chen, L.; Huang, X. *Phys. Rev. B* **2003**, *68*, 195108.
(5) Chung, S.-Y.; Bloking, J. T.; Chiang, Y.-M. *Nat. Mater.* **2002**, *1*, 123−128.
(6) He, H.; Liu, Y.; Liu, Q.; Li, Z.; Xu, F.; Dun, C.; Ren, Y.; Wang, M.-x.; Xie, J. *J. Electrochem. Soc.* **2013**, *160*, A793−A804.
(7) Xu, F.; He, H.; Liu, Y.; Dun, C.; Ren, Y.; Liu, Q.; Wang, M.-x.; Xie, J. *J. Electrochem. Soc.* **2012**, *159*, A678−A687.
(8) Malik, R.; Abdellahi, A.; Ceder, G. *J. Electrochem. Soc.* **2013**, *160*, A3179−A3197.
(9) Love, C. T.; Korovina, A.; Patridge, C. J.; Swider-Lyons, K. E.; Twigg, M. E.; Ramaker, D. E. *J. Electrochem. Soc.* **2013**, *160*, A3153−A3161.
(10) Boesenberg, U.; Meirer, F.; Liu, Y.; Shukla, A. K.; Dell'Anna, R.; Tyliszczak, T.; Chen, G.; Andrews, J. C.; Richardson, T. J.; Kostecki, R. *Chem. Mater.* **2013**, *25*, 1664−1672.
(11) Bai, P.; Cogswell, D. A.; Bazant, M. Z. *Nano Lett.* **2011**, *11*, 4890−4896.
(12) Gu, L.; Zhu, C.; Li, H.; Yu, Y.; Li, C.; Tsukimoto, S.; Maier, J.; Ikuhara, Y. *J. Am. Chem. Soc.* **2011**, *133*, 4661−4663.
(13) Kao, Y.-H.; Tang, M.; Meethong, N.; Bai, J.; Carter, W. C.; Chiang, Y.-M. *Chem. Mater.* **2010**, *22*, 5845−5855.
(14) Nishimura, S.-i.; Kobayashi, G.; Ohoyama, K.; Kanno, R.; Yashima, M.; Yamada, A. *Nat. Mater.* **2008**, *7*, 707−711.
(15) Ramana, C. V.; Mauger, A.; Gendron, F.; Julien, C. M.; Zaghib, K. *J. Power Sources* **2009**, *187*, 555−564.
(16) Padhi, A. K.; Nanjundaswamy, K. S.; Goodenough, J. B. *J. Electrochem. Soc.* **1997**, *144*, 1188−1194.
(17) Andersson, A. S.; Thomas, J. O. *J. Power Sources* **2001**, *97*−*98*, 498−502.
(18) Laffont, L.; Delacourt, C.; Gibot, P.; Wu, M. Y.; Kooyman, P.; Masquelier, C.; Tarascon, J. M. *Chem. Mater.* **2006**, *18*, 5520−5529.
(19) Delmas, C.; Maccario, M.; Croguennec, L.; Le Cras, F.; Weill, F. *Nat. Mater.* **2008**, *7*, 665−671.
(20) Zhang, W.-J. *J. Power Sources* **2011**, *196*, 2962−2970.

(21) Gibot, P.; Casas-Cabanas, M.; Laffont, L.; Levasseur, S.; Carlach, P.; Hamelet, S.; Tarascon, J.-M.; Masquelier, C. *Nat. Mater.* **2008**, *7*, 741−747.
(22) Meethong, N.; Kao, Y.-H.; Carter, W. C.; Chiang, Y.-M. *Chem. Mater.* **2009**, *22*, 1088−1097.
(23) Rodriguez, M. A.; Van Benthem, M. H.; Ingersoll, D.; Vogel, S. C.; Reiche, H. M. *Powder Diffraction* **2010**, *25*, 143−148.
(24) Sharma, N.; Guo, X.; Du, G.; Guo, Z.; Wang, J.; Wang, Z.; Peterson, V. K. *J. Am. Chem. Soc.* **2012**, *134*, 7867−7873.
(25) Chen, Z.; Ren, Y.; Qin, Y.; Wu, H.; Ma, S.; Ren, J.; He, X.; Sun, Y. K.; Amine, K. *J. Mater. Chem.* **2011**, *21*, 5604−5609.
(26) Dahn, J. R.; Zheng, T.; Liu, Y.; Xue, J. S. *Science* **1995**, *270*, 590−593.
(27) Dahn, J. R. *Phys. Rev. B* **1991**, *44*, 9170−9177.
(28) Wang, X.-L.; An, K.; Cai, L.; Feng, Z.; Nagler, S. E.; Daniel, C.; Rhodes, K. J.; Stoica, A. D.; Skorpenske, H. D.; Liang, C.; Zhang, W.; Kim, J.; Qi, Y.; Harris, S. J. *Sci. Rep.* **2012**, *2*, 747.
(29) Meethong, N.; Kao, Y.-H.; Tang, M.; Huang, H.-Y.; Carter, W. C.; Chiang, Y.-M. *Chem. Mater.* **2008**, *20*, 6189−6198.
(30) Wang, X.-J.; Jaye, C.; Nam, K.-W.; Zhang, B.; Chen, H.-Y.; Bai, J.; Li, H.; Huang, X.; Fischer, D. A.; Yang, X.-Q. *J. Mater. Chem.* **2011**, *21*, 11406−11411.
(31) Yamada, A.; Koizumi, H.; Nishimura, S.-i.; Sonoyama, N.; Kanno, R.; Yonemura, M.; Nakamura, T.; Kobayashi, Y. *Nat. Mater.* **2006**, *5*, 357−360.
(32) Bramnik, N. N.; Bramnik, K. G.; Baehtz, C.; Ehrenberg, H. *J. Power Sources* **2005**, *145*, 74−81.
(33) Orikasa, Y.; Maeda, T.; Koyama, Y.; Murayama, H.; Fukuda, K.; Tanida, H.; Arai, H.; Matsubara, E.; Uchimoto, Y.; Ogumi, Z. *Chem. Mater.* **2013**, *25*, 1032−1039.
(34) Allen, J. L.; Jow, T. R.; Wolfenstine, J. *Chem. Mater.* **2007**, *19*, 2108−2111.
(35) Chen, G.; Song, X.; Richardson, T. J. *Electrochem. Solid-State Lett.* **2006**, *9*, A295−A298.
(36) Delacourt, C.; Poizot, P.; Tarascon, J.-M.; Masquelier, C. *Nat. Mater.* **2005**, *4*, 254−260.
(37) Meethong, N.; Huang, H.-Y. S.; Carter, W. C.; Chiang, Y.-M. *Electrochem. Solid-State Lett.* **2007**, *10*, A134−A138.
(38) Yamada, A.; Koizumi, H.; Sonoyama, N.; Kanno, R. *Electrochem. Solid-State Lett.* **2005**, *8*, A409−A413.
(39) Orikasa, Y.; Maeda, T.; Koyama, Y.; Murayama, H.; Fukuda, K.; Tanida, H.; Arai, H.; Matsubara, E.; Uchimoto, Y.; Ogumi, Z. *J. Am. Chem. Soc.* **2013**, *135*, 5497−5500.